

This article was downloaded by:

On: 8 April 2010

Access details: *Access Details: Free Access*

Publisher *Taylor & Francis*

Informa Ltd Registered in England and Wales Registered Number: 1072954 Registered office: Mortimer House, 37-41 Mortimer Street, London W1T 3JH, UK



Aerosol Science and Technology

Publication details, including instructions for authors and subscription information:

<http://www.informaworld.com/smpp/title~content=t713656376>

Optical Properties of Organic-based Aerosols Produced by Burning Vegetation

Robert A. Sutherland ^a; Raj K. Khanna ^b

^a Atmospheric Research Division, U.S. Army Atmospheric Sciences Laboratory, White Sands Missile Range, NM ^b Department of Chemistry and Biochemistry, University of Maryland, College Park, MD

First published on: 01 January 1991

To cite this Article Sutherland, Robert A. and Khanna, Raj K. (1991) 'Optical Properties of Organic-based Aerosols Produced by Burning Vegetation', *Aerosol Science and Technology*, 14: 3, 331 – 342, First published on: 01 January 1991 (iFirst)

To link to this Article: DOI: 10.1080/02786829108959495

URL: <http://dx.doi.org/10.1080/02786829108959495>

PLEASE SCROLL DOWN FOR ARTICLE

Full terms and conditions of use: <http://www.informaworld.com/terms-and-conditions-of-access.pdf>

This article may be used for research, teaching and private study purposes. Any substantial or systematic reproduction, re-distribution, re-selling, loan or sub-licensing, systematic supply or distribution in any form to anyone is expressly forbidden.

The publisher does not give any warranty express or implied or make any representation that the contents will be complete or accurate or up to date. The accuracy of any instructions, formulae and drug doses should be independently verified with primary sources. The publisher shall not be liable for any loss, actions, claims, proceedings, demand or costs or damages whatsoever or howsoever caused arising directly or indirectly in connection with or arising out of the use of this material.

Optical Properties of Organic-based Aerosols Produced by Burning Vegetation

Robert A. Sutherland*

Atmospheric Research Division, U.S. Army Atmospheric Sciences Laboratory, White Sands Missile Range, NM 88002

Raj K. Khanna

Department of Chemistry and Biochemistry, University of Maryland, College Park, MD 20742

The real and imaginary refractive indexes of organic-based nonvolatile aerosols produced by burning vegetation are reported for the infrared spectral region. The data were obtained by an iterative Kramers-Kronig analysis of the transmission spectra (2–25 μm) obtained from thin-film samples deposited on a KBr substrate immersed directly in the smoke plumes of small-scale test fires. The results include samples from fires fueled by lawn grass, alfalfa, mesquite, tumbleweed, pine needles, and mixed twigs, leaves, and weeds. The most significant characteristics of all spectra are as follows: (a) strong absorptions in the 3–5- μm region owing to condensed water and CH_3/CH_2 groups of aliphatic hydrocarbons; (b) characteristic peaks in the 6-, 8-, and 10- μm regions owing to skeletal modes of aromatic and terpenic groups; and (c) relatively little absorption in the 10–12- μm region. The imaginary

refractive index of all samples is comparable (~ 0.10 – 0.30) in the 3–5- and 8–10- μm regions and is 3–10 times lower in the 10–12- μm region. In the 3–5- μm region, most of the absorption takes place in the interval between 3 and 4 μm as opposed to the 4–5- μm interval which shows significantly less absorption. It is also noteworthy that there is insignificant absorption in the 2.0–2.5- μm window region. Results are significantly different from values for elemental carbon which are known to be relatively wavelength independent in these spectral regions and of magnitude between ~ 0.50 and 1.0 for the imaginary index. Theoretical calculations, assuming particle sizes in the Rayleigh scattering regime, yields a mass extinction coefficient (m^2/g) for the organic smokes on the order of ~ 0.20 for the 8–10- μm region and as high as 0.40 at 3 μm to near zero at 5 μm in the 3–5- μm window.

INTRODUCTION

In studies of atmospheric aerosols it is usual to separate the carbonaceous constituents into two major components: one accounting for elemental, or “graphitic,” carbon (also called black carbon, or carbon black) and the other accounting for organic carbon. The elemental carbon component is the major constituent of what is commonly referred to as “soot,” although by practical definition soot may also contain significant amounts of other substances, including organic components. Both elemental carbon and soot are highly absorbing at wavelengths from the

visible through the infrared and, as a consequence, are manifested by a blackened appearance in smoke plumes. The organic carbon component is considerably more complicated than the elemental counterpart and is, as the name implies, composed of many different types of complex organic compounds, some of which may exist as organic vapors and others that may either attach to other smoke constituents, including soot particles, or may condense into oil-like droplets. These type aerosols, unlike the elemental counterparts, are usually nonabsorbing at the visible wavelengths and are manifested by a whitened appearance in smoke plumes (as also are water droplets and certain other aerosols).

*To whom correspondence should be addressed.

TABLE 1. Brief Listing of Major Chemical Types Found in Vegetative Fire Smokes

Chemical type	%C
Aromatic hydrocarbons	36
<i>n</i> -Alkanes	35
Branched alkanes	3
Alkenes	4
Terpenes/terpenoids	11
<i>n</i> -Alkanols	4

It is customary to further separate the organic component into the two categories of volatile (organic vapors) and nonvolatile (also called residual carbon in the smoke jargon). Going even further, Eatough et al. (1989) consider a semivolatile component. Over the years researchers have also found traces of a wide variety of other types of compounds in vegetative fire smokes, including namely, nitrates, sulfates, and phosphates, in Chaparral fires (Cofer et al., 1988). Other studies have identified traces of halogens, salts, and metals in wood smokes (Rau, 1989), and still others have identified metals and silicates in airborne ash (Weinman et al., 1981). Two other constituents of passing general interest are potassium, which is used as a tracer of wood fire smokes (Andreae, 1983; Calloway et al., 1989), and polycyclic aromatic hydrocarbons (PAH), which are of environmental concern (Dragoescu and Friedlander, 1989). In other studies, Kaaijak (1986) and Sutherland and Khanna (1987) presented evidence for the existence of terpenes and terpenoids in vegetative fire smokes, which is in part corroborated by Standley and Simoneit (1987), who have identified abietic acid and dehydroabietic acid as tracers of vegetative fire smokes. Other studies have identified numerous chemical compounds traceable to vegetative fire smokes in ambient atmospheric aerosols, including raindrops, at various stations over the world. A thorough discussion of these chemical types and their ultimate effects on the atmosphere is well beyond the scope of the work here; how-

ever, for more information the reader is referred to other sources (Simoneit and Mazurek, 1982, 1989; Standley and Simoneit, 1987).

In one of our own earlier cooperative field experiments conducted in Europe, Kaaijak (1986) identified over 60 chemical compounds in medium-sized vegetative test fires from grab samples collected near the fire source. The results from this test, summarized in terms of chemical types, are listed in Table 1.

The listing in Table 1 is by no means inclusive and is intended only as a guide for convenience in interpreting later results. In practice, the actual abundances of the various organic types are quite variable and will certainly differ somewhat from those shown in Table 1. There is, in fact, considerable variation even in considering only the total elemental and organic components. For example, in one study Dod et al. (1989) report that for burning plywood, elemental carbon makes up ~ 50–75% of the particulate contribution to the total emission factor (i.e., the emission factor is defined as the ratio of the mass of a particular constituent emitted to the total mass of fuel consumed) for both open and restricted ventilation conditions in medium-scale controlled experiments. In another study, Rau (1989) reports that, for well-ventilated "hot" burning flame wood fires, elemental carbon accounts for ~ 55–75% of the total carbon emission factor but, for poorly ventilated or "cool"-burning smoldering wood fires, the situation is reversed as organic carbon accounts for ~ 95% of the total. Dasch and Cadle (1989) report that for the Detroit area, the largest carbon source is residential wood-burning, which accounts for 60% of organic carbon emissions and 49% of elemental carbon emissions. Other values reported in the literature for vegetative fires usually fall within these extremes.

In modeling the effects of carbonaceous aerosols on the atmospheric optical (and ra-

diative) properties, researchers often ignore the organic component entirely and assume the underlying aerosol to be adequately represented by the elemental component (Chylek et al., 1981). In some cases this assumption may be valid, but, in the general case, one must also consider the more complex organic component. Although there is a range of uncertainty in selecting values appropriate for atmospheric studies, measurements of the refractive indexes for the elemental component are available (Twitty and Weinman, 1971). For vegetative-based fire smokes, however, one must also include the more illusive organic component for which data on the refractive indexes are much more difficult to find. In some of our previous work we have attempted to fill this void through measurements on laboratory-grade samples of the various chemical compounds associated with fire smokes (Sutherland and Khanna, 1987). In later sections we will have occasion to refer back to some of these data; however, for the most part this paper is focused on our most recent and more straightforward approach through the analysis of in situ samples collected directly in the plumes of small-scale test fires.

The findings are germane to at least two topical areas: first, studies of the effect of such aerosols on the earth-atmosphere radiative balance and hence climate alteration, and secondly, studies of the effect on remote sensing sensors and military systems that use the all important atmospheric windows for a variety of airborne and ground-based applications.

METHODOLOGY

The measurement method consists of five parts: (a) collection of the samples in the field, (b) laboratory measurements to determine the raw sample transmission spectra, (c) determination of sample thickness, (d) correction for Fresnel reflection at the various sample cell interfaces, and (e) mathe-

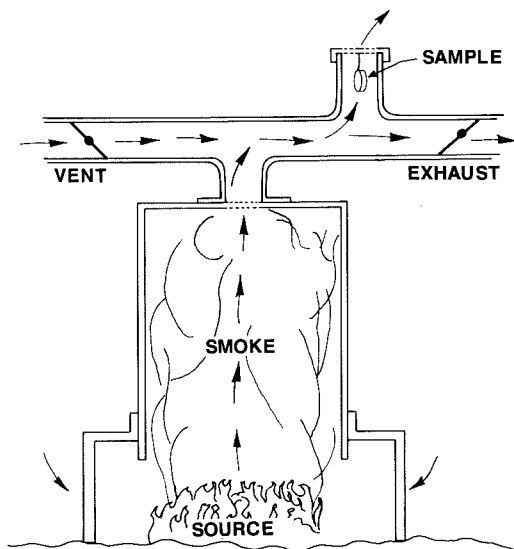


FIGURE 1. Sketch of the smoke sampling apparatus.

tical analyses to extract the complex refractive indexes from the sample transmittance spectra using a Kramers-Kronig analysis.

Sample Preparation

The samples were collected in the field using various configurations and adaptations of the apparatus sketched in Figure 1. The entire apparatus is operated outdoors and consists of a commercially purchased oil drum inverted and placed vertically over the fire source to channel the smoke to the sampling chamber. The drum is mounted ~50 cm above the fire to allow ventilation from the surroundings in through the bottom. The channeled smoke passes through an opening in the top of the drum into a horizontally mounted, 10-cm diameter escape vent. The samples are collected on circular KBr ($n \sim 1.56$) substrates, or optical "end windows," suspended in a vertically oriented and open-ended sampling vent attached to the escape vent (Figure 1). Prior to use, the KBr substrates (~5 cm in diameter and 1 cm thick)

were polished optically flat using a 600-grit pumice and then cleaned with alcohol; otherwise no other preparations of the substrate were required. Throughout the course of acquiring a sample, the outlet vent (Figure 1) was adjusted to limit, and to some extent control, the smoke density in the sample area. In this configuration it would take ~30–45 min to collect a sample a few micrometers thick, which was about optimal for the transmission measurements. In all cases the fires produced a thick, nearly white, smoke with a slight yellow-brown hue nearest the flame. The smokes all had a strong acrid odor characteristic of vegetative fire smokes. In practice, the samples appeared as an oil-like yellow-hued film deposited on both sides of the substrate. After deposition, the samples and substrate were transported intact to the laboratory for analysis. In the laboratory, one side of the substrate was cleansed of any sample material leaving only a one-layered sample-substrate configuration to be considered in the transmission analysis. This two-layer configuration is the most preferred and commonly used for this type of experiment.

Transmission data

The transmission measurements were made with a Perkin-Elmer Corp. (Norwalk, Conn.) model 1800 Fourier transform infrared spectrometer (FTIR) operated over a spectral interval from 5000 to 400 cm^{-1} (2–25 μm) at a resolution of $\sim 1 \text{ cm}^{-1}$. The measurements were made directly from the samples as collected on the KBr substrates used in the field. For each sample, the raw transmission signal was corrected for background and normalized to a reference, or baseline, signal obtained by fitting through points of maximum transmission significantly removed from absorption peaks. Plots of the corrected and normalized transmission, $T^*(\nu)$, for four samples—alfalfa, mixed weeds, lawn grass, and abietic

acid—are reproduced in Figures 2–5 and are discussed in more detail in later sections.

Sample Thickness

The first step in the analysis of the transmission data is to obtain an accurate measure of the sample thickness, d . If the film is uniformly flat and if the substrate refractive index is significantly different from that of the sample, then the channel fringes provide an extremely accurate method for measuring the film thickness. Unfortunately, neither of these conditions were met in this work; consequently, an alternate method was adopted. The spectrum of synthetic abietic acid liquid was recorded in a cell of known thickness from which the extinction coefficients were determined using standard procedures. The spectral characteristics of abietic acid are similar to those of the smoke films, especially in the CH_3/CH_2 stretching mode region in and around 3 μm . The sample film thickness was then estimated by calibrating on the CH_3/CH_2 peaks assuming the extinctions coefficients for abietic acid. An independent check was made by weighing the KBr substrate before and after removing a portion of the sample. The thickness was then calculated using a bulk density of 0.90 g/cm^3 , which is characteristic of many plant oils. This method yielded thickness estimates that were consistently 15–25% higher than those obtained using the CH_3/CH_2 peaks.

Fresnel Reflection

The next step is to account for effects of Fresnel reflection losses at the various air, sample, and substrate interfaces. The transmission signal appropriate for propagation through a sample film of thickness d (refractive indices $n = n_f$; $k = k_f$) deposited on a nonabsorbing substrate ($n = n_s$; $k_s = 0$) immersed in air ($n_a = 1$; $k_a = 0$) is written, approximately, as (Khanna et al., 1988; Os-

pina et al., 1988) as shown below in Eq. (1), where I_s represents the actual transmitted signal and I_b represents the baseline signal. The algebraic factor in brackets accounts, approximately, for Fresnel reflection losses at the various interfaces of the sample-cell system, α_f is the sample absorption coefficient and, as before, d represents the sample film thickness.

The higher-order terms in Eq. (1) account for all possible multiple reflections at the sample-cell interfaces and are included here for completeness, although the actual effects on the results were found to be negligible in comparison with other uncertainties. It is possible to derive a rigorous expression to account for the higher-order terms although the resultant algebraic equations are quite cumbersome (cf. Sill et al., 1980; Warren, 1986). In our sensitivity studies we found that for a worst-case example using a sample thickness of 1 μm and a wavelength of 25 μm , the error due to the higher-order terms is no larger than 2% as compared with errors of 15–25% in sample thickness. For thicker samples or shorter wavelengths the resultant errors were found to be even smaller.

In Eq. (1) the factors R_1, R_2, R_3 represent the Fresnel reflectances at the air-sample, sample-substrate, and substrate-air interfaces, respectively, and are written in terms of the refractive indexes of the various sample-cell media using the well-known Fresnel expressions (cf. Bohren and Huffman, 1983):

Air-film Interface.

$$R_1 = \frac{(n_f - 1)^2 + k_f^2}{(n_f + 1)^2 + k_f^2} \quad R_1^* = \frac{(n_f - 1)^2}{(n_f + 1)^2}$$

Film - Substrate Interface.

$$R_2 = \frac{(n_f - n_s)^2 + k_f^2}{(n_f + n_s)^2 + k_f^2} \quad R_2^* = \frac{(n_f - n_s)^2}{(n_f + n_s)^2}$$

Substrate-Air Interface.

$$R_3 = R_3^* = \frac{(n_s - 1)^2}{(n_s + 1)^2}, \tag{2}$$

where we have made explicit use of the fact that $k_s = k_a = 0$ and $n_a = 1.0$. Note that the quantities denoted by the asterisk, which refer to the baseline signal, I_b , are obtained by setting $k_f = 0$.

Mathematical Analysis: Determination of n_f and k_f .

The method for extracting the sample complex refractive indexes (n_f and k_f) is started with a rough estimate for the extinction coefficient, $\alpha_f [= \alpha_f(\nu) \sim |\ln T^*|/d]$, from which an estimate of the imaginary refractive index is obtained through the definition:

$$k(\nu) = \alpha(\nu)/2\pi\nu. \tag{3}$$

With $k(\nu)$ [actually $k_f(\nu)$] so determined then an estimate for $n_f(\nu)$ is obtained through the (subtractive) Kramers-Kronig integral relationship written here in general form as:

$$n(\nu) = n(\nu_0) + \frac{2}{\pi} \text{Prin} \left[\int_0^\infty \frac{k(\nu')\nu' k(\nu)\nu}{\nu'^2 - \nu^2} - \frac{k(\nu')\nu' - k(\nu_0)\nu_0}{\nu'^2 - \nu_0^2} d\nu' \right] \tag{4}$$

where $\text{Prin}\{X\}$ denotes the Cauchy principle value. In writing Eq. (4), we have used a

$$T^* = \frac{I_s}{I_b} = \left[\frac{(1 - R_1)(1 - R_2)(1 - R_3)/(1 - R_2 R_3)}{(1 - R_1^*)(1 - R_2^*)(1 - R_3^*)(1 - R_2^* R_3^*)} + \text{higher-order terms} \right] e^{-\alpha_f d}, \tag{1}$$

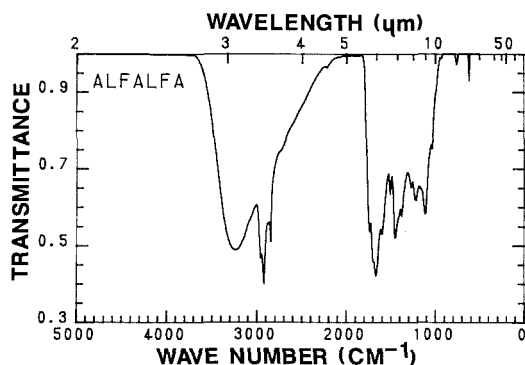


FIGURE 2. Transmittance spectrum of the alfalfa sample.

form suggested by Wood and Roux (1982) that is equivalent to the more conventional form but is computationally more efficient in treating the mathematical singularities. The actual evaluation of the integral does require care in order to avoid artifacts that could arise in the regions of singularities. The Kramers-Kronig method has been used successfully in the past by Hale and Querry (1973), Wood and Roux (1982), and Warren (1986).

These estimates for $n_f(\nu)$ and $k_f(\nu)$ are then used with Eqs. (1) and (2) to obtain a better estimate for $T^*(\nu)$ and hence $\alpha_f(\nu)$ and $k_f(\nu)$. The process, including the Kramers-Kronig analysis of Eq. (4), is continued until the values of n_f and k_f converge, which typically requires about four to five iterations. A key feature of this technique is that it takes into account the frequency (or wavelength) dependence of the reflection losses at the interfaces, a detail which, if overlooked, can cause serious errors in the determination of the extinction coefficients, especially in the regions of strong absorption.

RESULTS

Two examples of the normalized transmission spectra, $T^*(\nu)$, obtained from the alfalfa and mixed weed samples are shown in Figures 2 and 3. The data here have been corrected for instrumental effects and have

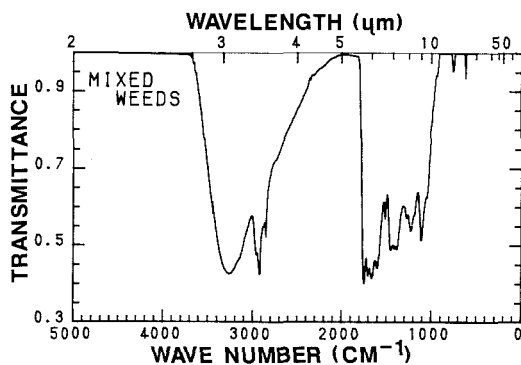


FIGURE 3. Transmittance spectrum of the weed-mix sample.

been normalized to unity using standard techniques. These results are typical of samples that were collected later into the project after we had made several practical improvements in the sampling technique that allowed thicker, more uniform films in a shorter sampling time. Some of the earlier samples were too thin to allow reliable analysis to extract the refractive indexes.

For all samples, including those of Figure 2 and 3, it was found that, as might be expected, regardless of specific source type, all spectra exhibited the same general features characteristic of complex organic compounds. It was also found, however, that there are both marked similarities (in general) and marked differences (in detail) from sample to sample. For example, in the mid-infrared region ($\sim 3000 \text{ cm}^{-1}$), all spectra showed the broad band absorption owing to O—H...O hydrogen-bonded groups centered near 3250 cm^{-1} and the three superimposed sharp absorption lines at 2950 , 2920 , and 2850 cm^{-1} to CH_2/CH_3 stretchings (Bellamy, 1975). Also, in the far infrared region beginning at $\sim 1800 \text{ cm}^{-1}$ and extending down to slightly $< 1000 \text{ cm}^{-1}$, all samples exhibit a complex structure that is, in general, similar from sample to sample but different in detail. Many of the features in this region can be associated with various molecular bonds known to absorb strongly in this region. For example, most of the region $< 1400 \text{ cm}^{-1}$ exhibits absorp-

tions resulting from skeletal C—C stretches and C—C—C, C—OH in plane and out of plane-bending vibrations. Other significant features are the two small isolated absorption peaks near 760 and 620 cm^{-1} owing to CH_3/CH_2 rocking and twisting modes.

It is significant for our applications that, for all samples, there is substantially less absorption in the far infrared window region $< \sim 1000\text{ cm}^{-1}$ than in the region above. This finding can be quite important in remote sensing work in that the data indicate that the $10\text{--}12\text{-}\mu\text{m}$ region might offer a better window for probing through such smokes than the more often used $8\text{--}12\text{-}\mu\text{m}$ window. It is also noteworthy that the two regions from 2500 to 2000 cm^{-1} ($4.0\text{--}5.0\text{ }\mu\text{m}$) and from 5000 to 4000 cm^{-1} ($2.0\text{--}2.5\text{ }\mu\text{m}$) are relatively void of strong absorption.

In the far infrared region, the two spectra of Figures 2 and 3 are again similar in that both show the rather sharp transitions defining the region of generally significant absorption beginning at $\sim 1800\text{ cm}^{-1}$ and ending at $\sim 1000\text{ cm}^{-1}$. There are several other points of similarity that are evidenced in Figures 2 and 3, such as the two sets of double peaks: one near 1500 cm^{-1} and the other near 1300 cm^{-1} and the two isolated absorptions mentioned earlier at 760 and 620 cm^{-1} . It is also significant, however, that there are noticeable differences as well as similarities in other details that are evident from inspection.

In Figure 4 we show another example obtained from a lawn grass sample which, as expected, is similar overall to the alfalfa and weed-mix samples although there are also differences. The sample used to generate the lawn grass data was collected in some of the earlier experiments which produced somewhat thinner films and hence higher bulk transmission than those of Figures 2 and 3. A significant difference in the lawn grass spectrum as compared to the alfalfa and weed-mix samples is the prominent absorption line at the leading edge of the far infrared region near 1750 cm^{-1} . The

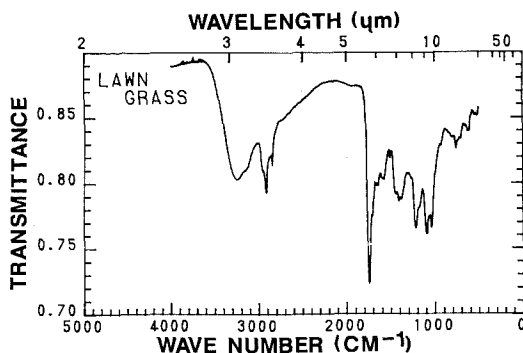
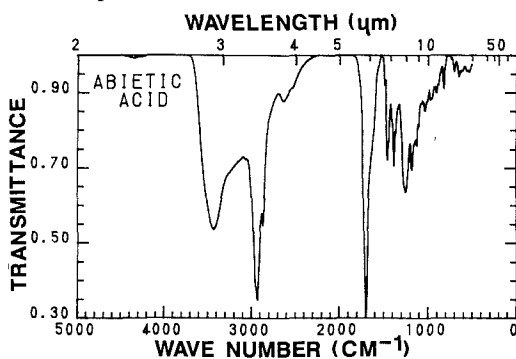


FIGURE 4. Transmittance spectrum of the lawn grass sample.

line can also be seen in the alfalfa and weed-mix samples but is relatively less prominent, especially in the alfalfa sample. In our experience we have observed that this particular spectral feature is a good indication of the presence of terpenes and terpenoids in the samples.

In order to demonstrate the effect of terpenes and terpenoids we show, in Figure 5, a spectrum obtained from a laboratory grade sample of abietic acid, which, as mentioned earlier, has been identified as a constituent of vegetative fire smokes. The overall similarities with the vegetative samples are fairly evident, as also are the differences. In particular, the acid sample shows the characteristic broad band and absorption peaks in the 3000-cm^{-1} region which is also evident in

FIGURE 5. Transmittance spectrum of the abietic acid sample.



all vegetative samples and in other terpenoids (Sutherland and Khanna, 1987). The differences in the far infrared region, however, are more marked although the overall similarity is also evident. In our studies of terpenes and terpenoids, we have found that the strong peak near 1750 cm^{-1} , which is prominent in the lawn grass sample and also present in all samples (some not shown) is somewhat unique to abietic acid. We have other ongoing work based upon laboratory grade samples that may shed more light on this topic in the future but which is beyond the scope of this paper.

Although we have traced down data in the literature that show transmission spectra of the various individual chemical compounds associated with fire smokes, we have very few direct measurements on real vegetative fire smokes to compare with those shown here. An exception, published in a fairly obscure source, is the work of Barrett et al. (1969) who used a KBr fiber filter to collect smoke samples produced from burning hay. The spectra from these older results are remarkably similar, qualitatively, to those reported here for alfalfa (Figure 2) and are, in fact, almost identical in essential overall features. The most significant difference is that the earlier work (Barrett et al., 1969) shows a small continuous background in the region $< 1000\text{ cm}^{-1}$ with two broad humps centered near 800 and 600 cm^{-1} . We believe that this difference which is also apparent in our earlier samples (Figure 4) can probably be ascribed to the small film thickness and lower spectral resolution in the earlier work. It is noteworthy that the region $< 1000\text{ cm}^{-1}$ is characterized by very weak CH_3/CH_2 absorptions that may be swamped by other sampling artifacts.

REFRACTIVE INDEXES

The real and imaginary refractive indexes of the alfalfa and weed-mix samples, which are more or less representative of the samples as a whole are plotted in Figure 6.

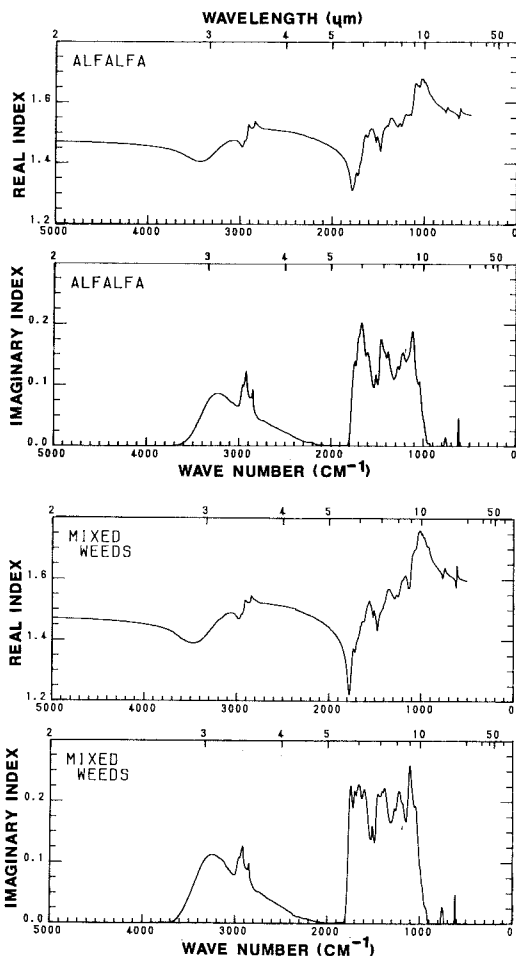


FIGURE 6. Real and imaginary refractive indexes for the alfalfa and weed-mix samples.

For these samples the real index has a nominal value near 1.50 and exhibits significant fluctuations as high as ~ 1.75 at the extreme maximum near 1000 cm^{-1} and as low as ~ 1.25 at the extreme minimum near 1800 cm^{-1} . These fluctuations are, of course, a consequence of the changing imaginary index as demanded by the Kramers-Kronig relationship of Eq. 4 used in the data analysis. The imaginary component for the alfalfa sample is generally lower than that of the weed-mix sample by $\sim 25\%$. This difference could be real but is more likely a manifestation of the measurement accuracy which is, for the most part, dominated by

TABLE 2. Numerical Listing of the Real and Imaginary Refractive Indexes of the Mixed Weed Sample Averaged over 25-cm⁻¹ Intervals

ν (cm ⁻¹)	$n(\nu)$	$k(\nu)$	ν (cm ⁻¹)	$n(\nu)$	$k(\nu)$	ν (cm ⁻¹)	$n(\nu)$	$k(\nu)$
5000	1.470	0.000E + 0	3500	1.389	0.425E - 1	2000	1.441	0.765E - 3
4975	1.470	0.117E - 5	3475	1.388	0.521E - 1	1975	1.434	0.856E - 3
4950	1.470	0.431E - 5	3450	1.389	0.616E - 1	1950	1.426	0.103E - 2
4925	1.469	0.712E - 5	3425	1.392	0.713E - 1	1925	1.417	0.122E - 2
4900	1.469	0.100E - 4	3400	1.395	0.812E - 1	1900	1.406	0.143E - 2
4875	1.469	0.130E - 4	3375	1.401	0.905E - 1	1875	1.392	0.167E - 2
4850	1.468	0.161E - 4	3350	1.409	0.986E - 1	1850	1.373	0.193E - 2
4825	1.468	0.194E - 4	3325	1.418	0.105E + 0	1825	1.345	0.225E - 2
4800	1.468	0.227E - 4	3300	1.427	0.109E + 0	1800	1.287	0.150E - 1
4775	1.468	0.262E - 4	3275	1.437	0.112E + 0	1775	1.230	0.118E + 0
4750	1.467	0.298E - 4	3250	1.447	0.113E + 0	1750	1.310	0.217E + 0
4725	1.467	0.335E - 4	3225	1.456	0.112E + 0	1725	1.367	0.196E + 0
4700	1.467	0.373E - 4	3200	1.464	0.109E + 0	1700	1.386	0.214E + 0
4675	1.466	0.414E - 4	3175	1.470	0.107E + 0	1675	1.413	0.220E + 0
4650	1.466	0.455E - 4	3150	1.475	0.105E + 0	1650	1.449	0.223E + 0
4625	1.466	0.499E - 4	3125	1.482	0.101E + 0	1625	1.462	0.207E + 0
4600	1.465	0.544E - 4	3100	1.487	0.944E - 1	1600	1.484	0.217E + 0
4575	1.465	0.590E - 4	3075	1.488	0.887E - 1	1575	1.518	0.193E + 0
4550	1.464	0.639E - 4	3050	1.488	0.839E - 1	1550	1.520	0.152E + 0
4525	1.464	0.690E - 4	3025	1.484	0.796E - 1	1525	1.488	0.145E + 0
4500	1.463	0.742E - 4	3000	1.475	0.804E - 1	1500	1.484	0.141E + 0
4475	1.463	0.797E - 4	2975	1.470	0.967E - 1	1475	1.442	0.167E + 0
4450	1.463	0.855E - 4	2950	1.483	0.108E + 0	1450	1.478	0.211E + 0
4425	1.462	0.915E - 4	2925	1.502	0.122E + 0	1425	1.498	0.210E + 0
4400	1.462	0.977E - 4	2900	1.526	0.976E - 1	1400	1.519	0.217E + 0
4375	1.461	0.104E - 3	2875	1.523	0.891E - 1	1375	1.549	0.217E + 0
4350	1.461	0.111E - 3	2850	1.533	0.876E - 1	1350	1.567	0.188E + 0
4325	1.460	0.118E - 3	2825	1.536	0.663E - 1	1325	1.557	0.168E + 0
4300	1.459	0.126E - 3	2800	1.530	0.579E - 1	1300	1.543	0.170E + 0
4275	1.459	0.134E - 3	2775	1.525	0.532E - 1	1275	1.544	0.186E + 0
4250	1.458	0.142E - 3	2750	1.521	0.513E - 1	1250	1.546	0.196E + 0
4225	1.457	0.150E - 3	2725	1.520	0.497E - 1	1225	1.574	0.215E + 0
4200	1.457	0.159E - 3	2700	1.520	0.471E - 1	1200	1.598	0.201E + 0
4175	1.456	0.169E - 3	2675	1.519	0.440E - 1	1175	1.610	0.185E + 0
4150	1.455	0.179E - 3	2650	1.518	0.412E - 1	1150	1.589	0.171E + 0
4125	1.454	0.190E - 3	2625	1.517	0.389E - 1	1125	1.580	0.225E + 0
4100	1.453	0.201E - 3	2600	1.515	0.367E - 1	1100	1.660	0.243E + 0
4075	1.453	0.213E - 3	2575	1.514	0.345E - 1	1075	1.694	0.203E + 0
4050	1.452	0.225E - 3	2550	1.513	0.322E - 1	1050	1.714	0.190E + 0
4025	1.451	0.239E - 3	2525	1.512	0.300E - 1	1025	1.754	0.149E + 0
4000	1.449	0.253E - 3	2500	1.511	0.277E - 1	1000	1.752	0.956E - 1
3975	1.448	0.268E - 3	2475	1.510	0.256E - 1	975	1.739	0.604E - 1
3950	1.447	0.284E - 3	2450	1.508	0.232E - 1	950	1.720	0.326E - 1
3925	1.446	0.302E - 3	2425	1.507	0.208E - 1	925	1.705	0.174E - 1
3900	1.444	0.321E - 3	2400	1.505	0.183E - 1	900	1.679	0.000E + 0
3875	1.443	0.341E - 3	2375	1.503	0.150E - 1	875	1.660	0.000E + 0
3850	1.441	0.363E - 3	2350	1.499	0.124E - 1	850	1.647	0.000E + 0
3825	1.439	0.387E - 3	2325	1.495	0.111E - 1	825	1.637	0.000E + 0
3800	1.437	0.413E - 3	2300	1.492	0.104E - 1	800	1.627	0.000E + 0
3775	1.434	0.443E - 3	2275	1.489	0.905E - 2	775	1.612	0.638E - 2
3750	1.432	0.476E - 3	2250	1.486	0.806E - 2	750	1.630	0.192E - 1
3725	1.428	0.514E - 3	2225	1.482	0.751E - 2	725	1.623	0.000E + 0
3700	1.424	0.573E - 3	2200	1.479	0.668E - 2	700	1.615	0.000E + 0

TABLE 2. (continued).

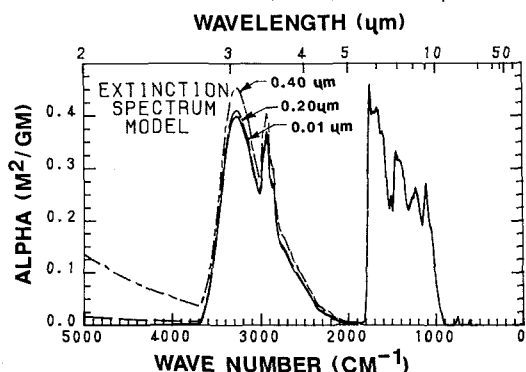
ν (cm ⁻¹)	$n(\nu)$	$k(\nu)$	ν (cm ⁻¹)	$n(\nu)$	$k(\nu)$	ν (cm ⁻¹)	$n(\nu)$	$k(\nu)$
3675	1.419	0.138E-2	2175	1.476	0.547E-2	675	1.609	0.000E+0
3650	1.414	0.414E-2	2150	1.472	0.424E-2	650	1.603	0.000E+0
3625	1.408	0.761E-2	2125	1.468	0.336E-2	625	1.600	0.147E-1
3600	1.403	0.127E-1	2100	1.463	0.267E-2	600	1.610	0.000E+0
3575	1.398	0.187E-1	2075	1.459	0.216E-2	575	1.602	0.000E+0
3550	1.394	0.257E-1	2050	1.453	0.150E-2	550	1.599	0.000E+0
3525	1.391	0.337E-1	2025	1.448	0.117E-2	525	1.596	0.000E+0

errors in the determination of the sample thickness. Results, averaged over 25-cm⁻¹ intervals, for the weed-mix sample, which we consider most representative for vegetative smokes in general, are listed in Table 2.

As an exercise to demonstrate the significance of the findings on the optical effects that such organic aerosols may have in applications we have used the Mie scattering theory to calculate the aerosol mass extinction coefficient (m²/g) spectrum that might exist in applications. The results, shown in Figure 7, were obtained using the FORTRAN program published by Bohren and Huffman (1983). For demonstration purposes we have assumed spherical aerosols of bulk density 0.90 g/cm³, typical of plant oils, and have made the calculations for droplet diameters of 0.01, 0.20, and 0.40 μ m. As is evident from Figure 7 the results for the smaller droplets (0.01 and 0.20 μ m) are nearly independent of droplet size. For the most part

the extinction spectra tracks closely with the imaginary index spectrum especially at the lower wavenumbers and smaller size droplets. These results are not surprising in a qualitative sense and are, in fact, indicative of extinction in the long wavelength regime which is dominated by absorption (as opposed to scattering). The result for 0.40 μ m is slightly above the Rayleigh regime as indicated by the added scattering most evident at wavenumbers $> \sim 3000$ cm⁻¹. In the far infrared region the extinction is completely dominated by absorption and the results follow the imaginary index spectrum almost precisely for all droplet sizes. Particles on the order of 0.10 μ m or smaller are most likely for vegetative fires according to measurements by Pinnick et al. (1982) and indirect determinations by Uthe et al. (1982). For wood fire smokes Helspar et al. (1980) report mean particle diameters from ~ 0.01 to 0.12 μ m, and, for smoldering wood fires, Mulholland and Ohlemiller (1982) report geometric mean diameters of 0.20–0.30 μ m and mass median diameters of 2–3 μ m.

FIGURE 7. Calculated extinction spectrum based upon the measured weed-mix indexes for assumed aerosol diameters of 0.01, 0.20, and 0.40 μ m.



Some rough estimates based on the calculations of Figure 7 indicate that, on the average, the extinction coefficient in the 8–10- μ m region (~ 0.20) is somewhat larger than that in the 3–5- μ m region (~ 0.15) although the peak value in the 3–5- μ m region (~ 0.40) is larger than both. On the other hand, the average over the entire 8–12- μ m region is about half that of the 8–10- μ m region and of course, the average over the 10–12- μ m region is nearly negligible in comparison to the other bands. It is also significant that there is substantially

more absorption in the 3–4- than in the 4–5- μm interval. Obviously, in interpreting broadband, low resolution, measurements great care must be taken to define and account for details of the instrumental band-pass.

There have been attempts to determine broadband extinction ratios directly from transmission as measured through actual smoke plumes in the field. In some of our own cooperative field tests, we have estimated extinction coefficient ratios between the far (8–12 μm) and mid- (3–5 μm) infrared spectral bands from data obtained using the transmissometer system of Watkins et al. (1988). Some results obtained from transmission measurements through an actual small-scale smoke plume are shown in Figure 8 in the form of optical depth, or "Log T " correlation plots. From the slope of the plot we estimate a far-to-mid averaged extinction coefficient ratio of ~ 0.78 as opposed to the theoretical estimates of Figure 7, which yielded a somewhat lower value (~ 0.67). There are many reasons to not expect close agreement here but the results do give at least some feel as to the magnitude of the effects of other (perhaps more volatile) aerosols that probably exist in real smoke plumes but are not collected by our technique.

DISCUSSION AND SUMMARY

Infrared spectral measurements performed on bulk samples of smoke produced by burning vegetation indicate the existence of numerous organic compounds that produce complex, spectrally dependent, absorption in both the 3–5- and 8–14- μm atmospheric sensing windows. Spectra of samples from several different source types show similar overall results that, however, differ in detail especially in the 8–14- μm region. In the 3–5- μm region the absorption is dominated by three distinct absorption peaks in the 2900 cm^{-1} region that are superimposed on a broad band centered near 3250 cm^{-1} . The

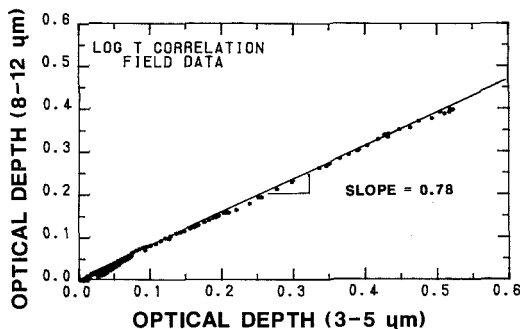


FIGURE 8. Log T correlation plot from mid- and far-infrared broadband field transmission measurements through a vegetative fire smoke plume.

average value of the imaginary index, k , is near 0.20 in the 8–10- μm region, and varies from a peak of ~ 0.40 at 3 μm to near zero at 5 μm in the 3–5- μm region. The imaginary index is near zero in both the 10–12- and 2.0–2.5- μm window regions.

Results of Mie calculations in the Rayleigh regime yield extinction coefficients on the order of 0.20 and 0.15 for the 3–5- and 8–10- μm regions, respectively. Results from field transmissometer tests indicate an extinction ratio of ~ 0.78 for the 8–12- and 3–5- μm bands as compared to a ratio of about 0.67 based on the Mie calculations. For submicrometer particles most of the extinction in the 3–5- μm region takes place in the 3–4- rather than the 4–5- μm interval. Extinction in the 10–12- μm portion of the far infrared atmospheric window is about a factor of 10 times lower than in the 8–10- μm portion. These latter results strongly suggest that the 10–12- μm region is significantly better for probing through these smoke types than the more commonly used 8–12- or 8–14- μm regions.

REFERENCES

- Andreae, M. O. (1983). *Science*. 220:1148–1151.
 Barrett, W. J., Dismukes, E. B., and Powell, J. B. (1969). *Southern Research Institute 2nd Annual Report*. Department of the Army Contract DAAA15-68-C-0154, Defense Technical Information Center AD No. 506023.

- Bellamy, L. J. (1975). *The Infrared Spectra of Complex Molecules*. John Wiley & Sons, New York.
- Bohren, C. F., and Huffman, D. R. (1983). *Absorption and Scattering of Light by Small Particles*. John Wiley & Sons, New York.
- Calloway, C. P., Li, S., Buchanan, J. W., and Stevens, R. K. (1989). *Atmos. Environ.* 23:67-69.
- Chylek, P., Ramaswamy, V., Cheng, R., and Pinnick, R. G. (1981). *Appl. Opt.* 20:2980-2985.
- Cofer, W. R., Levine, J. S., Sebacher, D. I., Winstead, E. L., Riggan, P. J., Brass, J. A., and Ambrosia, V. G. (1988). *J. Geophys. Res.* 93:5207-5212.
- Dasch, J. M., and Cadle, S. H. (1989). *Aerosol Sci. Technol.* 10:236-248.
- Dod, R. L., Brown, N. J., Mowrer, F. W., Novakov, T., and Williamson, R. B. (1989). *Aerosol Sci. Technol.* 10:20-27.
- Dragoescu, C., and Friedlander, S. (1989). *Aerosol Sci. Technol.* 10:249-257.
- Eatough, D. J., Sedar, B., Lewis, L., Hansen, L. D., and Farber, R. J. (1989). *Aerosol Sci. Technol.* 10:438-449.
- Hale, G. M., and Querry, M. R. (1973). *Appl. Opt.* 12:555-562.
- Helsper, C., Fissan, H. J., Muggli, J., and Scheidweiler, A. (1980). *J. Aerosol Sci.* 11:439-446.
- Kaaijk, J. (1986). "Chemical Characterization of Fire Products," Technical Report Number PML 1986, Prins Maurits Laboratorium, Institute for Chemical and Technological Research, TNO, The Hague, Netherlands.
- Khanna, R. K., Ospina, M. J., and Zhao, G. (1988). *Icarus*. 73:527-535.
- Mulholland, G., and Ohlemiller, T. J. (1982). *Aerosol Sci. Technol.* 1:59-71.
- Ospina, M., Zhao, G., and Khanna, R. K. (1988). *Spec-trochim. Acta*. 44A:23-26.
- Pinnick, R. G., Fernandez, G., and Hines, B. D. (1982). Unpublished manuscript, U.S. Army Atmospheric Sciences Laboratory, White Sands Missile Range, NM.
- Rau, J. A. (1989). *Aerosol Sci. Technol.* 10:181-192.
- Sill, G., Fink, U., and Ferraro, J. R. (1980). *J. Opt. Soc. Am.* 70:724-739.
- Simoneit, B. R. T., and Mazurek, M. A. (1982). *Atmos. Environ.* 16:2139-2159.
- Simoneit, B. R. T., and Mazurek, M. A. (1989). *Aerosol Sci. Technol.* 10:267-291.
- Standley, L. J., and Simoneit, B. R. T. (1987). *Environ. Sci. Technol.* 21:163-169.
- Sutherland, R. A., and Khanna, R. K. (1987). In *Abstracts of the 1987 Annual Meeting of the American Association for Aerosol Research*, University of Washington, Seattle, September 1987.
- Twitty, J. T., and Weinman, J. A. (1971). *J. Appl. Meteorol.* 10:725-731.
- Uthe, E. E., Morley, B. M. and Nielsen, N. B. (1982). *Appl. Opt.* 21:460-463.
- Warren, S. G. (1986). *Appl. Opt.* 25:2650-2674.
- Watkins, W. R., Kantrowitz, F. T., and Crow, S. B. (1988). *Soc. Photo-Opt. Instrum. Eng.* 926:69-84.
- Weinman, J. A., Harshvardhan, and Olson, W. S. (1981). *Appl. Opt.* 20:199-206.
- Wood, B. E., and Roux, J. A. (1982). *J. Opt. Soc. Am.* 72:720-728.

Received March 19, 1990; accepted September 4, 1990.